Dynamic Crystallography Reveals Early Signaling Events in Ultraviolet Photoreceptor UVR8

Xiaoli Zeng[1#], Zhong Ren[2#], Qi Wu[3], Jun Fan[3], Pan-Pan Peng[1], Kun Tang[1], Ruiqin Zhang[3], Kai-Hong Zhao[1*] and Xiaojing Yang[4,5*]

[1] Key State Laboratory of Agricultural Microbiology, Huazhong Agricultural University, Wuhan, Hubei 430070, China

[2] Renz Research Inc., Westmont, IL 60559, USA

[3] Department of Physics and Materials Science, City University of Hong Kong, Kowloon, Hong Kong

[4] Department of Biochemistry and Molecular Biology, The University of Chicago, Chicago, IL 60637, USA

[5] Department of Chemistry, The University of Illinois at Chicago, Chicago, IL 60607, USA.

***To whom correspondence should be addressed:**
Xiaojing Yang, Department of Chemistry, University of Illinois at Chicago, 845 West Taylor Street, Chicago, IL 60607, USA. Email. xiaojing@uic.edu. Tel. 312-413-9406.

Kai-Hong Zhao, Key State Laboratory of Agricultural Microbiology, Huazhong Agricultural University, Wuhan, China. Email. khzhao@163.com

[#]These authors contribute to this work equally.

Keywords: photoreceptor; light signaling; dynamic crystallography; UVR8; photo-perception mechanism

Fig. S1

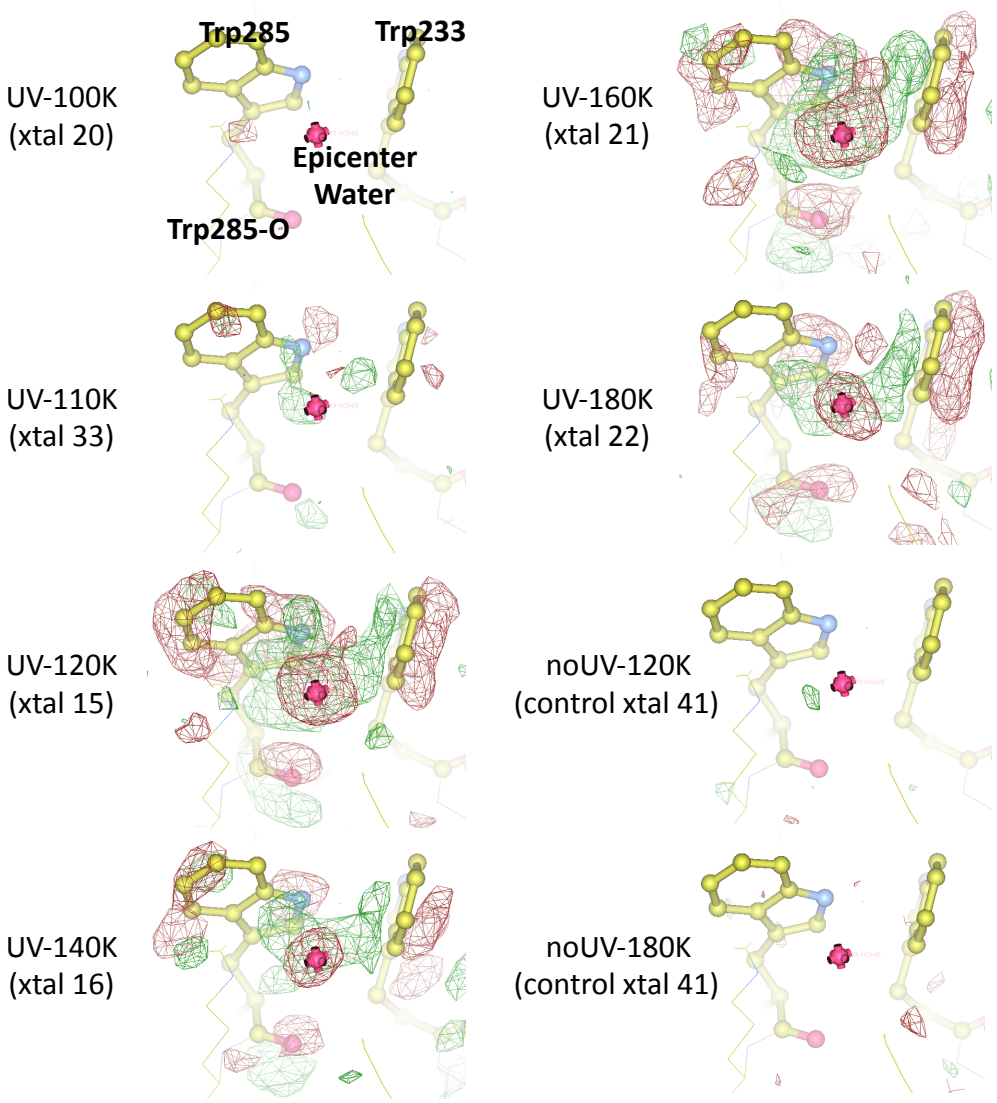

Fig. S1. Raw difference (F_{UV}-F_{Dark}) maps from temperature-scan (T-scan) experiments. Difference densities near the epicenter in subunit B (contoured at +/-3σ; positive in green, negative in red) are shown. Strong difference densities start to appear when the temperature rises above 110 K, and they are largely consistent between 120 and 180 K. Significant map features are associated with the indole rings of Trp285 and Trp233, the carbonyl oxygen of Trp285 (Trp285-O) and the epicenter water. Such features are absent in two control experiments conducted at 120 and 180 K, at which no UV-B irradiation was applied. Note that datasets used in generating a difference map were collected from two different volumes of the same crystal. This data collection strategy is designed to reduce effects due to X-ray radiation damage and crystal-to-crystal variation, which is critically important for extracting weak yet reliable difference signals from dynamic crystallographic experiments. See also Fig. S2.

Fig. S2

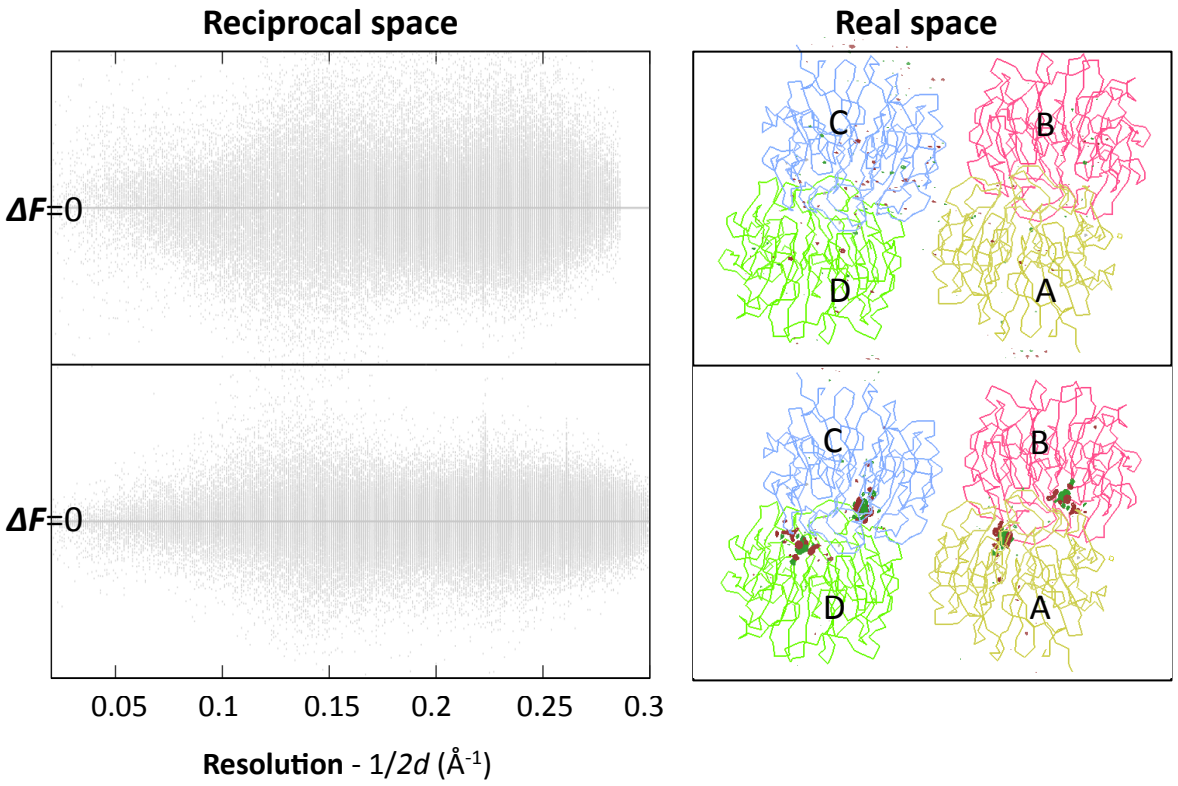

Fig. S2. Difference signals reciprocal space (left) and real space (right). Difference signals in reciprocal space are represented as difference structure factor amplitudes (***ΔF***) as function of resolution in scatter plots. Gray straight lines mark the positions where ***ΔF***=0. Difference signals in real space are shown in difference electron densities (contoured at ±4.5σ) of the entire asymmetric unit containing four subunits (A, B, C and D). Positive densities in green and negative negative densities in red. **Top:** difference signals were obtained from two dark sets (corresponding to WT-15 and WT-16 in Table S1). **Bottom:** difference signals were obtained between the paired dark and UV datasets from the same crystal (WT-15). ***ΔF*** ***(F_{UV}-F_{Dark})*** from the the same crystal displays a rather tight and symmetrical distribution around ***ΔF***=0, which gives rise to strong and localized difference densities at the dimer interface in both the A/B and C/D dimers. On the other hand, ***ΔF*** between two dark data sets from different crystals indeed shows no interpretable difference densities in real space, although their distribution around ***ΔF***=0 is wider in reciprocal space, most likely due to crystal-to-crystal variations (Table S1). We conclude: **1)** difference densities in the ***(F_{UV}-F_{dark})*** difference map are indeed resulted from UV-induced structural changes; **2)** Difference signals in reciprocal space are largely buried in random noises. So it is imperative to collect both light and reference data sets from the same crystal to obtain the best possible signal-to-noise ratio in real space.

Fig. S3

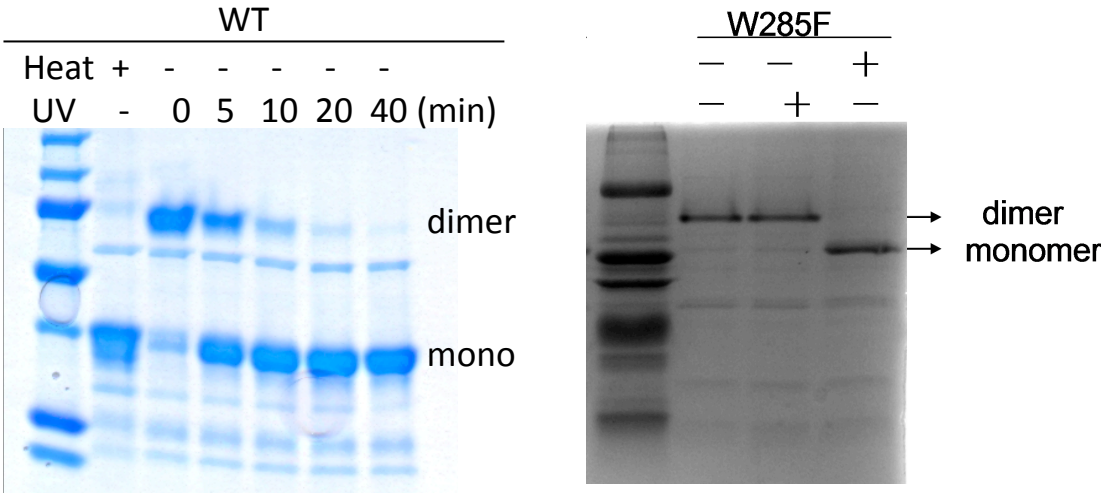

Fig. S3. Photo-activity of wild type (WT) and the W285F mutant of *At*UVR8. a) UV-B-induced dimer dissociation in WT *At*UVR8. Protein samples of equal amount were subjected to heat treatment at 95°C (lane 2) or UV-B irradiation for various durations ranging from 0 to 40 minutes (lane 3-7) before loading into an SDS-PAGE gel. Lane 1 is the molecular weight markers. The dimer-to-monomer ratio markedly decreases with duration of UV-B irradiation. **b)** The W285F dimer did not readily dissociate after applying 5-min UV-B irradiation.

Fig. S4

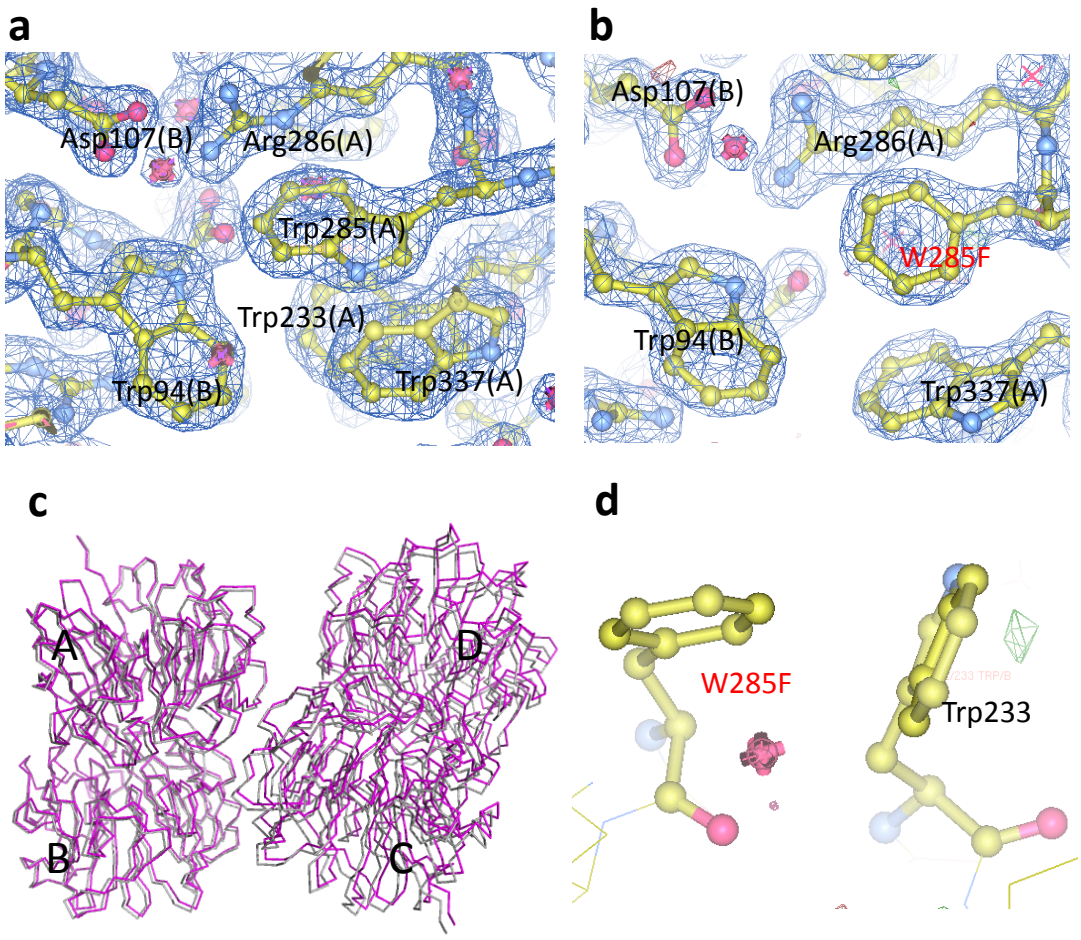

Fig. S4. Crystal structures of WT and W285F. a) The 2***F***o-***F***c map (contoured at 1.3σ) near the epicenter of the *At*UVR8 dark structure at 1.67 Å resolution. Well-defined electron densities are associated with residues at the epicenter including Trp285, Trp233 and Trp337 from subunit A and Trp94 from subunit B. Arg286A and Asp107B form double salt bridges across the dimer interface. **b)** 2***F***o-***F***c map of W285F at 1.8 Å resolution near the mutation site. **c)** Superposition between the Cα traces of two dark structures shows slightly different crystal packing. The dark structure for a typical crystal used for T-scan experiments is in gray. The dark structure used for capturing the I_{180K} structure is in magenta. Four subunits forming two biological dimers are labeled as A/B and C/D, respectively. **d)** ($\boldsymbol{F}_{UV}$-$\boldsymbol{F}_{Dark}$) difference map of W285F at 120K shows no significant light-induced structural changes. Difference densities (contoured at +/-3σ) are shown near the W285F mutation site.

Fig. S5

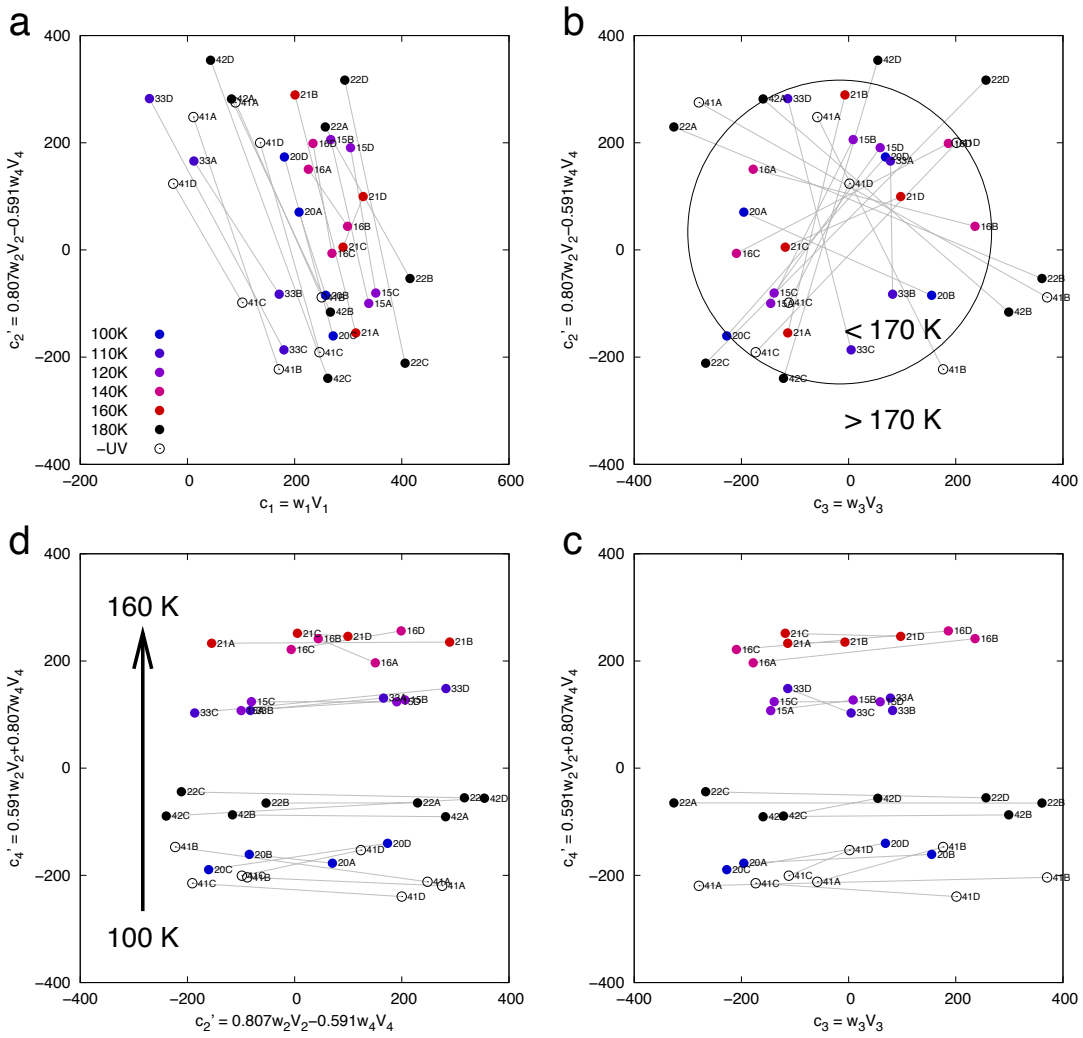

Fig. S5. SVD analysis of difference maps and temperature dependence of light-induced structural changes. Each solid dot corresponds to an $\boldsymbol{F}_{UV}$-$\boldsymbol{F}_{Dark}$ difference map associated with each subunit of *At*UVR8. Colors from cool to warm represents temperature from 100 to 160 K; 180 K is colored in black. Open circles represent difference maps from control experiments with no UV irradiation applied. Scatter plots in panels a, b, and c show relative compositions of SVD-decomposed maps in an orthogonal space of the top four most significant dimensions (c_1 through c_4). Subspace c_2-c_4 is rotated by an angle of 36.2° and the resulting subspace c_2'-c_4' is shown in panel d. Strong temperature dependency is observed along c_4' from 100 to 160 K (panel d), and along dimension c_1 (panel a). These temperature-dependent trends suggest that as a major species decays, a minor structural species accumulates with temperatures above 120 K. Two control datasets (-UV in open circles) are clustered with 100 K, which confirms the absence of signals. Difference maps at 180 K are drastically different, suggesting a major structural event between 160 and 180 K. Two subunits of the same biological dimer are connected by gray lines. The longer the gray line, the more distinct between two subunits. At 180 K, such differences between subunits are significantly larger as all black dots are outside the circle while all colored dots are inside (panel b). Random orientations of these connecting lines indicate that although early structural changes are very similar in all subunits, later structural events associated with dimer dissociation are rather asymmetric.

Fig. S6

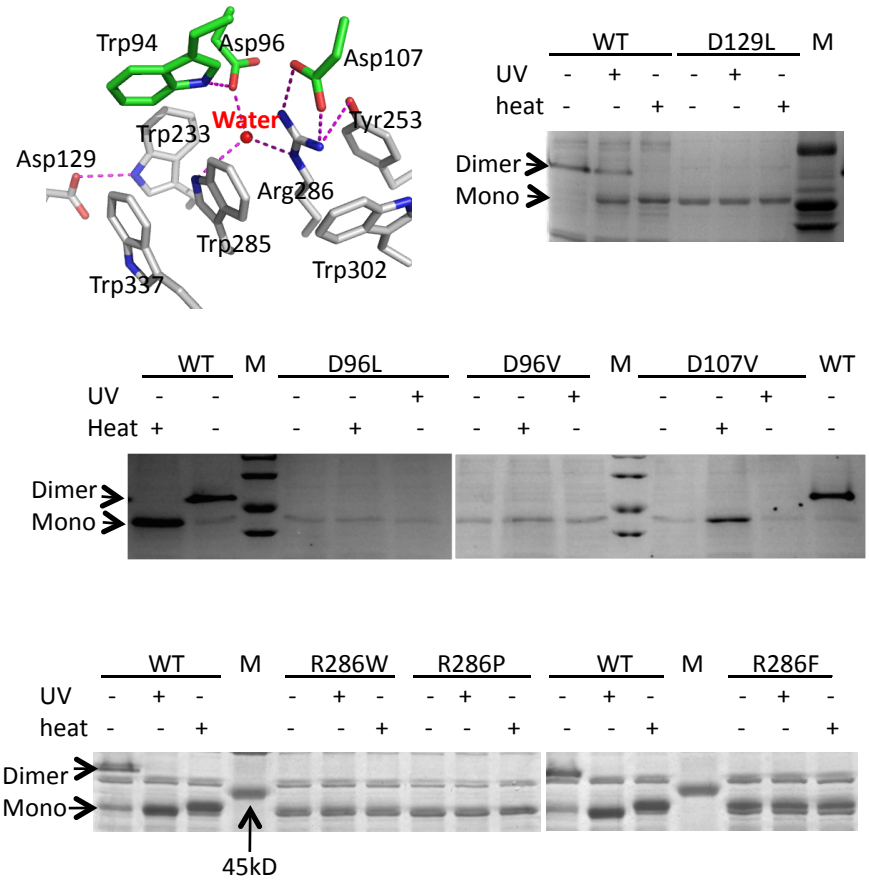

Fig. S6. Residues in the vicinity of the epicenter probed by mutagenesis. Top-left: key interactions (dashed line) near the epicenter at the dimer interface (subunit A in gray; B in green). The epicenter water is represented by a red sphere. SDS-PAGE of WT and mutant samples were subjected to heat treatment (95°C for 10 mins) or UV-B irradiation for 20 mins or none. Samples were obtained via two-step purification (Ni^{2+}-affinity and size exclusive chromatography), except those in the bottom panel which were directly eluted from a Ni^{2+}-affinity column. Mutation that directly or indirectly alter the network of hydrogen bonds and salt bridges near the epicenter water are more prone to monomerization compared to WT.

Fig. S7

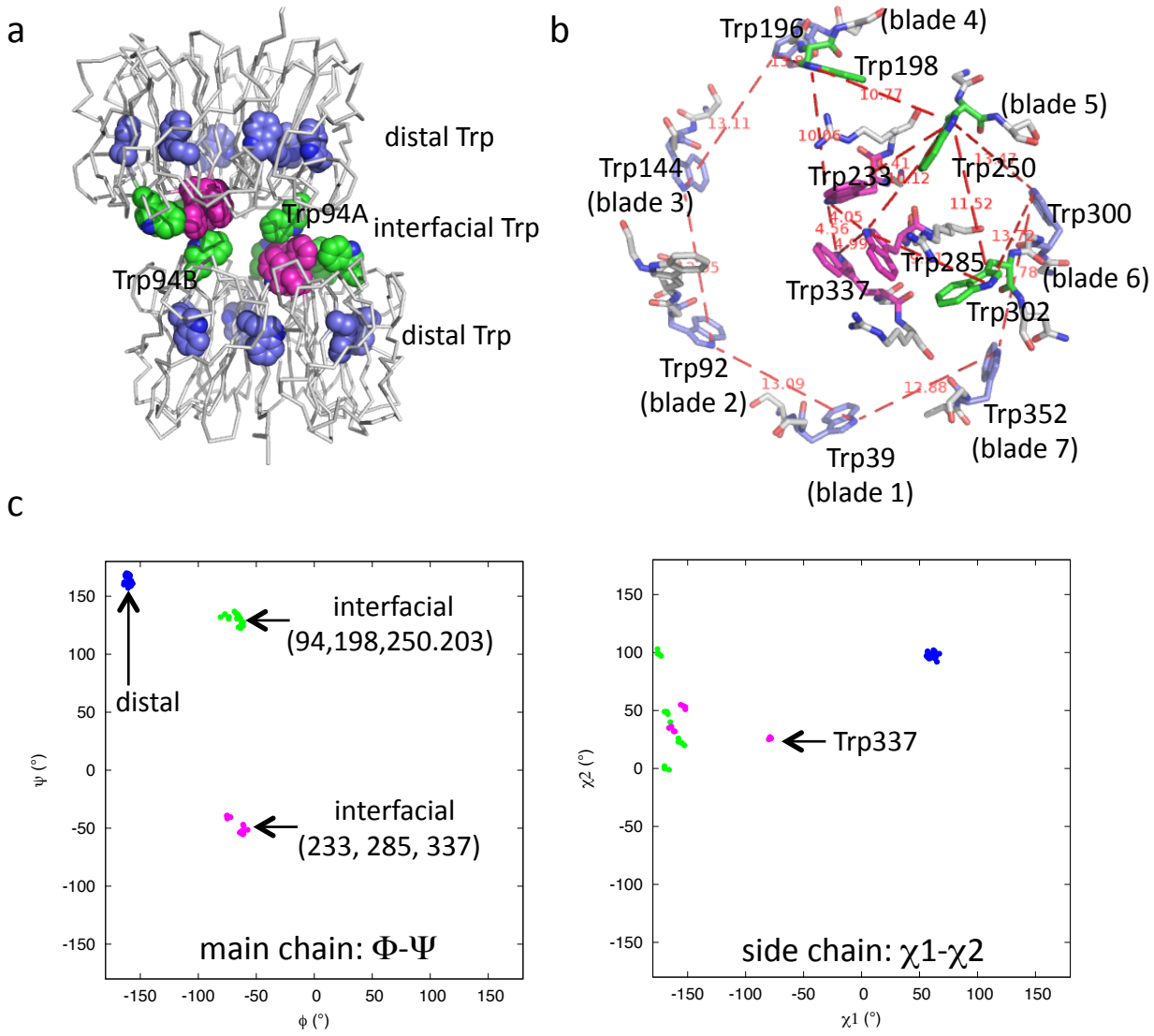

Fig. S7. Spatial and conformational distributions of Trp residues in the *At*UVR8 structure. a) Distal Trp (39, 92, 144, 196, 300, 352 in blue) and interfacial Trp (94, 198, 250, 302 in green and 233, 285, 337 in magenta). Trp residues are denoted based on their spatial locations relative to the dimer interface. **b)** Inter-Trp distances within a monomer (measured between two indole nitrogen atoms) are labeled along red dashed line in the top-down view from the dimer interface. Distal Trp residues are ~13 Å apart from one another, while the interfacial Trp are clustered. **c)** Scatter plots of the backbone torsional angles Φ-Ψ (left panel) and rotamer torsional angles χ1-χ2 (right panel). The color scheme is the same as in a) and b). Distal Trp residues share very similar backbone and rotamer conformations. Interfacial Trp residues adopt two distinct backbone conformation, distinguished by Trp(233, 285, 337) at the epicenter and Trp(94,198,250,302) at the peripheral.

Fig. S8

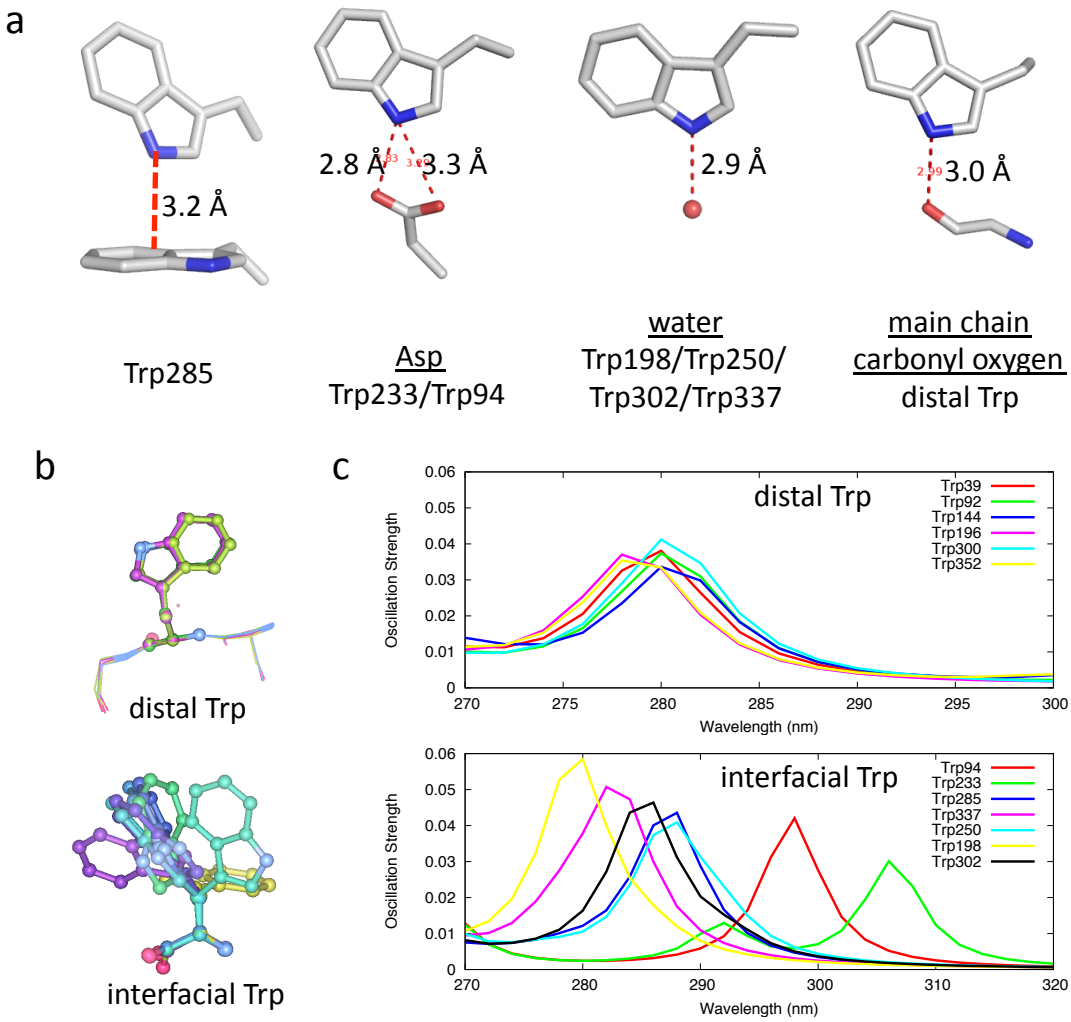

Fig. S8. Protein environment, conformational distribution and optical properties of Trp residues in *At*UVR8. **a)** 13 Trp residues are involved in four types of interactions via the indole nitrogen. **b)** Structural alignment of distal Trp residues with flanking Gly residues (top) shows nearly identical backbone and rotamer conformations. Alignment of interfacial Trp residues displays diverse rotamer orientations (bottom). **c)** Individual absorption spectra in the wavelength range of 270-320nm for distal (top) and interfacial (bottom) Trp residues are derived from the TD-DFTB calculations based on the dark structure of *At*UVR8 (PDB ID: 4NAA).

Fig. S9

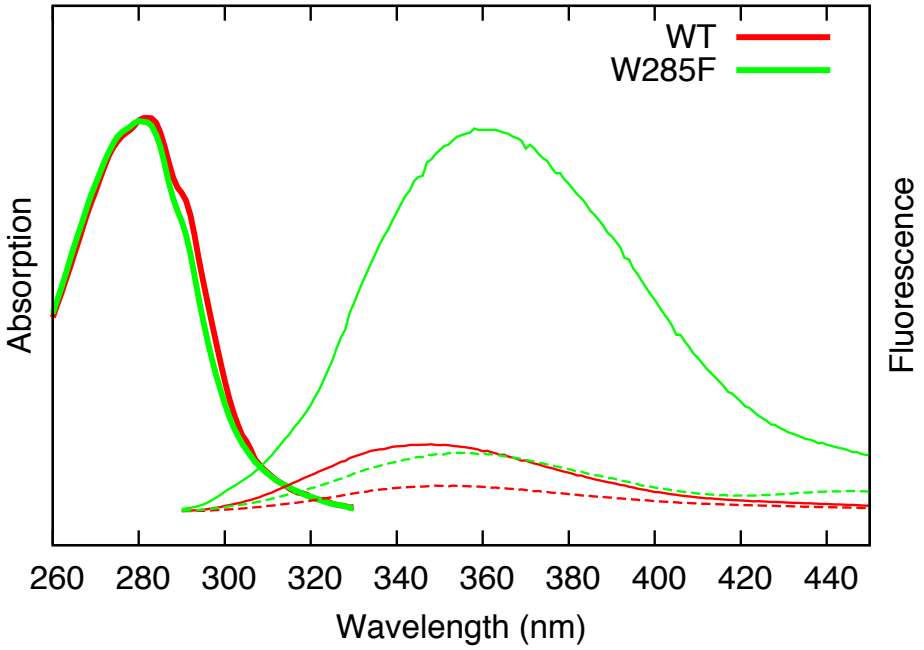

Fig. S9. Absorption (thick lines) and fluorescence emission (thin lines) spectra of WT (red) and W285F (green). Solid and dashed thin lines represent the emission spectra measured before and after UV irradiation at 256nm for 0.5 hour, respectively. Concentrations of protein samples were adjusted to OD_{280nm} = 0.12. The excitation wavelength for the fluorescence measurements was set at 280nm. The fluorescence emission in W285F was significantly increased (~5-6 fold) compared to WT, with the emission peak shifted from 345nm to 360nm.